The Journal of Chemical Physics

# Measurements and characterization of the dynamics of tracer particles in an actin network

Cite as: J. Chem. Phys. **154**, 144901 (2021); https://doi.org/10.1063/5.0045278
Submitted: 25 January 2021 • Accepted: 18 March 2021 • Published Online: 12 April 2021

Maayan Levin, Golan Bel and Yael Roichman

The Journal of Chemical Physics ARTICLE scitation.org/journal/jcp

# Measurements and characterization of the dynamics of tracer particles in an actin network

Cite as: J. Chem. Phys. 154, 144901 (2021); doi: 10.1063/5.0045278
Submitted: 25 January 2021 • Accepted: 18 March 2021 •
Published Online: 12 April 2021



Maayan Levin,[1] Golan Bel,[2] and Yael Roichman[3,a)]

## AFFILIATIONS

[1] Raymond and Beverly Sackler School of Chemistry, Tel Aviv University, Tel Aviv 6997801, Israel
[2] Department of Solar Energy and Environmental Physics, Blaustein Institutes for Desert Research, Ben-Gurion University of the Negev, Sede Boqer Campus 8499000, Israel
[3] Raymond and Beverly Sackler School of Physics and Astronomy, Tel Aviv University, Tel Aviv 6997801, Israel

[a)] **Author to whom correspondence should be addressed:** roichman@tauex.tau.ac.il

## ABSTRACT

The underlying physics governing the diffusion of a tracer particle in a viscoelastic material is a topic of some dispute. The long-term memory in the mechanical response of such materials should induce diffusive motion with a memory kernel, such as fractional Brownian motion (fBM). This is the reason that microrheology is able to provide the shear modulus of polymer networks. Surprisingly, the diffusion of a tracer particle in a network of a purified protein, actin, was found to conform to the continuous time random walk type (CTRW). We set out to resolve this discrepancy by studying the tracer particle diffusion using two different tracer particle sizes, in actin networks of different mesh sizes. We find that the ratio of tracer particle size to the characteristic length scale of a bio-polymer network plays a crucial role in determining the type of diffusion it performs. We find that the diffusion of the tracer particles has features of fBm when the particle is large compared to the mesh size, of normal diffusion when the particle is much smaller than the mesh size, and of the CTRW in between these two limits. Based on our findings, we propose and verify numerically a new model for the motion of the tracer in all regimes. Our model suggests that diffusion in actin networks consists of fBm of the tracer particle coupled with caging events with power-law distributed escape times.



## I. INTRODUCTION

The blooming of fluorescence single particle microscopy in the past few decades has provided bountiful data of single entities undergoing stochastic motion in biological and bio-inspired materials.[1–6] The goal of these experiments, as well as the accompanying theoretical works, is to learn about the characteristics of the medium in which the motion takes place and about the dynamics of the tracer particles in the usually crowded and disordered medium. These data reflect multiple aspects of the biological systems, such as the processes governing their fluctuations in space, their structure, and their mechanical properties. In a more general context, single particle tracking has numerous applications, including the measurement of interaction potentials[7] and hydrodynamic interactions,[8,9] as well as characterization of numerous non-equilibrium processes.[10–13]

Successful toolkits for analysis of tracer motion were developed in the context of random processes leading to anomalous diffusion.[5,14,15] In this context, the diffusion of a tracer particle is characterized by the diffusion exponent, $\alpha$. The diffusion exponent is defined by the time dependence of the mean squared displacement (MSD), MSD $\sim \tau^{\alpha}$, where $\tau$ is the duration of the tracer motion. We note that a concentrated effort to provide tools for efficient and accurate characterization of the diffusion type in more realistically constrained conditions is underway. New approaches for data analysis include, for example, machine learning,[16–20] Bayesian statistics,[21] and power spectrum analysis.[22]

Generally speaking, in thermal equilibrium, the diffusion of a tracer particle in a dense, complex medium is either normal or sub-diffusive, that is, $\alpha$ is equal to or lower than 1, respectively. Sub-diffusion was observed in a verity of complex systems, for example, biological systems[23–25] such as living cells,[26–28] liquid crystals,[29,30] and geological systems.[31,32] Very different mechanisms can induce a sub-diffusive behavior (i.e., $\alpha < 1$) including confinement, transient trapping, and memory in the mechanical response of the environment.[5,33–36] These mechanisms lead to different classes of diffusion processes such as random walk on a fractal structure (RWF),[37–39] continuous time random walk (CTRW),[40–42] and fractional Brownian motion (fBm).[43–45] The MSD and its functional dependence on lag time serve as a main tool to distinguish different diffusive processes and the underlying physical processes that lead to them.

In order to validate, adapt, and improve the available analysis tools, especially for use in biological systems, they need to be implemented on relevant well-controlled model systems. One candidate for such a model system is a material made of a network of the biopolymer actin, which is the most abundant protein in the cytoskeleton of eukaryotic cells. Actin creates networks in the cell, at many length scales and with different structures, which can be reproduced by selecting the polymerization buffer and the protein composition *in vitro*.[46–55] Actin networks have been characterized extensively, both in terms of their mechanical properties[46,47,56,57] and their structure.[58,59]

The motion of tracer particles in actin networks was also studied to some extent.[60,61] It is expected that tracer particles with a radius, $a$, much smaller than the mesh size of the network, $\xi$, will diffuse normally ($\alpha = 1$). This is expected since the tracer particles can pass easily between filaments and are mainly sensitive to the local viscous environment.[62] The main effect of the actin network is an increased viscosity, which results in a smaller diffusion coefficient. When $a \geq \xi$, the particles are expected to be confined to a finite region of the network with small movements within this region and due to the dynamics of the actin. For the case of $a \approx \xi$, the particles are expected to sub-diffuse, thereby reflecting the elasticity and structure of the network.

Anomalous diffusion, $\alpha \neq 1$, has been widely observed by single particle tracking microscopy in complex systems. For living systems, such as the cytoplasm, the motion of the tracer particles was found to belong to the fBM class.[63–66] This type of diffusion was also found in synthetic crowded fluids,[67,68] polymers,[36,64,69] and computer simulations of these.[70,71] In the context of microrheology, it was proven that the viscoelastic properties of a material can be inferred from the motion of a tracer particle within it. Viscoelasticity entails a long-term memory in the response of a material to mechanical perturbations, which should be reflected in an fBM-type diffusive motion of a tracer particle. In the case of polymer networks, microrheology provides accurate characterization when the tracer particles are larger than the expected mesh size[72] and are influenced by a memory formed by frequent contact with the elastic network.

This understanding is in discrepancy with a surprising result observed in an *in vitro* actin network, where the tracer particles were found to conform to the continuous time random walk (CTRW) type of diffusion.[60] In this pioneering work,[60] the motion of tracer particles was studied as a function of the ratio between the mesh size of the network and the tracer particles' radius. In intermediate values of $a/\xi$ (0.3–1), it was suggested that the tracer particle motion belongs to the CTRW class based on the heavy tail escape time distribution when hopping between "cages." While such a hopping mechanism was considered theoretically,[73] with a potential energy barrier between cages, it predicts normal diffusion in the asymptotic limit rather than CTRW (due to the finite moments of the escape time distribution in this case).

Here, we attempt to shed light on the mechanisms governing the dynamics of tracer particles within a polymer network as a function of the ratio between the particle size and the network's mesh size ($a/\xi$).

We perform single particle tracking experiments of colloidal tracer particles in entangled actin networks. We study the tracer dynamics in actin networks with various monomer concentrations and use two different sizes of the tracer particles. The recorded dynamics are analyzed extensively in terms of ergodic properties, probability density functions, and temporal and spatial correlations. The analysis is performed for the entire range of the tracer radius to mesh size ratio $0.26 \leq a/\xi \leq 1$. We find that as $a/\xi$ increases, the diffusion type changes from normal to CTRW-like to fBm. We suggest a model explaining the range of transport modes and show that the simulated trajectories resemble the observed ones.

## II. MATERIALS AND METHODS

### A. Materials

G-actin was purified from rabbit skeletal muscle acetone powder,[74] with a gel filtration step, stored on ice in G-buffer (5 mM Tris HCl, 0.1 mM $CaCl_2$, 0.2 mM ATP, 1 mM DTT, 0.01% $NaN_3$, and pH 7.8), and used within two weeks. G-actin concentration was determined by absorbance using a UV/visible spectrophotometer (Ultraspec 2100 pro, Pharmacia) in a cuvette with a 1 cm path length and an extinction coefficient of $\varepsilon_{290} = 26\,460\ M^{-1}\ cm^{-1}$. Polystyrene colloids with radius of a = 0.75 $\mu$m (Polysciences, Catalog No. 09719-10) and a = 0.25 $\mu$m (Invitrogen, lot 1173396) were incubated for 2 h before the experiment began with a 10 mg/ml bovine serum albumin (BSA) solution (Sigma) to prevent nonspecific binding of protein to the bead surface.[75] Actin polymerization was initiated by adding G-actin in various concentrations to F-buffer solution (5 mM Tris HCl, 1 mM $MgCl_2$, 0.05M KCl, 200 $\mu$M EGTA, and 1 mM ATP) and gently mixing it. The colloidal particles were added before mixing. The actin monomer concentration varied between $C_A$ = 2–27 $\mu$M corresponding to a mesh size range of $\xi$ = 0.95–0.28 $\mu$m.[76]

### B. Sample preparation

Samples were prepared on glass coverslips (40 mm in diameter) coated with methoxy-terminated PEG (Polyethylene glycol, Mw = 5000 g/mol, Nanocs) for 2 h before the experiment began to prevent F-actin filaments from sticking to the glass surface. The sample chamber was ~150 $\mu$m high and sealed with paraffin wax. Actin polymerization was carried out by mixing the monomers, buffer, and the fluorescent tracer particles together. After mixing, the suspensions were placed on the sample holder, and the sample was sealed. The recording was started only after polymerization ended and the network reached steady-state conditions according to Ref. 77. In order to avoid wall effects, imaging was carried out at a distance of ~60 $\mu$m from the glass. The resulting F-actin networks are

well described as networks of semi-flexible polymers,[78–82] and their mesh size, $\xi = 0.3/\sqrt{c_a}$,[76] was easily controlled by controlling the initial monomer concentration $c_a$ ($c_a$ in mg/ml and $\xi$ in $\mu$m). This relation was checked by us[59] and is well accepted in the field.[83–86] The range of concentration values that we used corresponds to a mesh size range of $\xi = 0.95$–$0.28$ $\mu$m, thereby enabling $0.79 \le a/\xi < 2.68$ for the $a = 0.75$ $\mu$m beads and $0.26 \le a/\xi \le 0.89$ for the $a = 0.25$ $\mu$m beads.

### C. Fluorescence microscopy and imaging

Imaging the motion of the tracer particles within the suspensions was carried out using an Olympus IX71 epi-fluorescence microscope at $\lambda = 480$ nm with a 40× air objective for a = 0.75 $\mu$m particles and at $\lambda = 605$ nm with a 60× oil objective for a = 0.25 $\mu$m particles. We recorded the motion of ~250 particles in the field of view for ~6 min using a CMOS video camera (Grasshopper 3, Point Gray) at a frame rate of 30 Hz with an exposure time of 10 ms. We used data from at least $5 \cdot 10^4$ frames per experiment and repeated each experiment twice. Particle tracking was carried out by conventional video microscopy using the protocol of Crocker and Grier[87] implemented in MATLAB software. The distribution of the number of snapshots in each trajectory, $L_{traj}$, varies significantly between the samples; the higher the actin concentration, the longer the average trajectory length. We used over 2000 trajectories for most of our analysis and at least 750 trajectories; the analysis is based on trajectories satisfying $L_{traj} > 500$.

## III. RESULTS AND DISCUSSION

In our experiments, we tuned the ratio between a and $\xi$ over a range of $0.26 \le a/\xi \le 1$. We then imaged the motion of the tracer particles embedded in the actin network under steady-state conditions and extracted their trajectories. We observe marked differences between typical trajectories of particles in networks of different actin concentrations (Fig. 1). As expected, trajectories of the same length spread further out at low actin concentrations. As the actin concentration increases, the trajectories become more compact. For low a/$\xi$, the trajectories reflect almost normal diffusion since the probe particles can move easily through the network. At intermediate a/$\xi$, the particles are mostly constrained by the network and jump between different micro-environments (or "cages") infrequently. As the dimensions of the particles increase with respect to the mesh size, the particles get more restricted by the network, and a movement between cages becomes less likely.

In order to characterize the diffusion mechanism at each network concentration and tracer particle size, we followed the methodology proposed in Ref. 5. The first test that we performed in order to classify the diffusion mechanism of the tracer particles within the actin networks was to extract their typical mean squared displacement averaged over the ensemble of particles, EA-MSD,

$$\langle \Delta \vec{r}^2(t) \rangle = \frac{1}{N_t} \sum_{k=1}^{N_t} (\vec{r}_k(t) - \vec{r}_k(0))^2, \tag{1}$$

where $\vec{r}_k(t)$ is the position of the $k$th particle at time $t$ and the average is over the ensemble of tracer particles in all similar experiments [Fig. 2(a)].

In our analysis, we assume (and verify) that the system is in a statistically steady-state, that is, its properties do not evolve over time. As shown in Fig. 2(a), for $0.26 \le a/\xi \le 0.4$, the EA-MSD is close to being linear with time, i.e., the particles exhibit normal diffusion. From the slope of the EA-MSD, in this region, we can extract the diffusion coefficient of the tracer particles. Using the Stokes–Einstein relation, we find that the effective viscosity of these networks is on the order of ~4 times larger than the viscosity of pure water. This is expected due to hydrodynamic interactions with the actin network[62,88,89] and the reduced diffusivity due to the obstacles set by the actin filaments.

As expected, at larger values of a/$\xi$, the EA-MSD exhibits anomalous sub-diffusion, increasing as a power-law for long times. We extract the diffusion power, $\alpha$, from the EA-MSD curves at long times [Fig. 2(b)]. We see that in the range of $0.26 < a/\xi < 0.89$, the tracer particle diffusion changes significantly. As a/$\xi$ increases, the

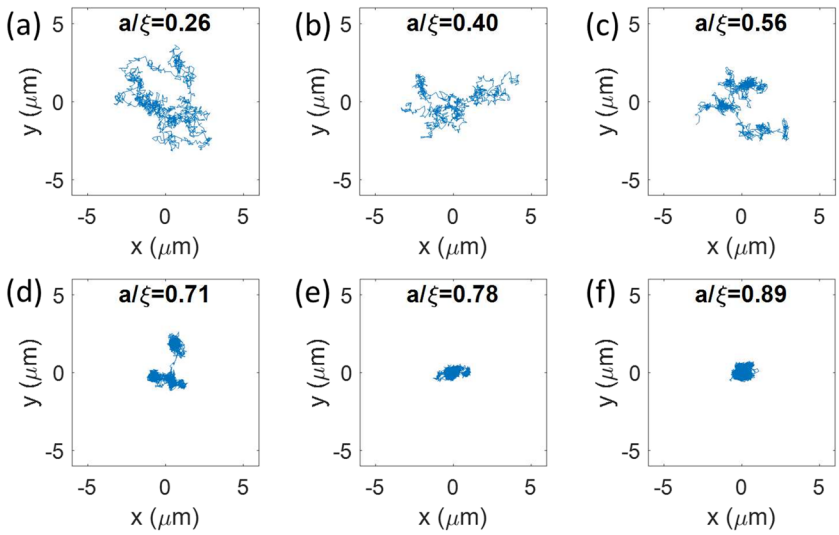


**FIG. 1**. Typical trajectories of tracer particles projected on the x–y plane for samples with increasing a/$\xi$. In (a) and (b), the prob particles show an almost normal diffusion; in (c) and (e), they are more constrained by the network but free to jump between different micro-environments; and in (f), the particles' movement is significantly restricted by the dense actin network.

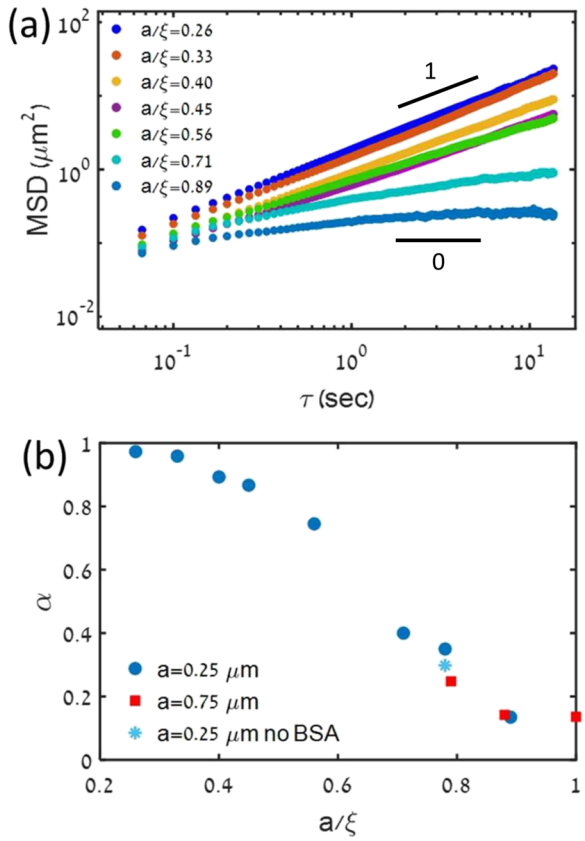


**FIG. 2.** (a) EA-MSD as a function of lag time for samples with different values of a/ξ and a tracer particle radius of a = 0.25 μm. The motion of the tracer particles becomes more confined as a/ξ increases. (b) The diffusion exponent, α, as a function of a/ξ measured for samples with two sizes of beads, a = 0.25 and 0.75 μm. The pale blue asterisk represents an experiment that was performed using beads that did not undergo surface treatment (see Sec. II B) corresponding to the experiments presented in Ref. 60.

particles become more confined, and the diffusion power decreases from ~1 to ~0.13. These results are in good agreement with those of previous reports.[60] To verify that the defining factor of the diffusion exponent is the ratio a/ξ, rather than the bead radius or the actin concentration, we compare results obtained by two sets of experiments: the first with tracer particles of radius a = 0.25 μm and the second with a = 0.75 μm. Both were performed over a large range of actin concentrations [Fig. 2(b)]. We find good agreement between the two sets of experiments, confirming that the ratio of the bead size to the mesh size dictates the diffusion type of the tracer particles. As shown in Fig. 2(b), in the range of $0.4 < a/\xi < 0.8$, the diffusion exponent strongly decreases. That sharp decrease is in accordance with the significant change in the individual trajectories of the tracer particles (see Fig. 1) in that range.

The next classification test is for ergodicity.[5] A main difference between the fBm and the CTRW is their ergodicity. It was shown that for a sub-diffusion CTRW (governed by a power-law tailed distribution of the escape time), the process is not ergodic;[90–92] that is, the time-average and the ensemble-average of physical observables are not the same even in the limit of a large ensemble and infinitely long trajectories. To this end, we compare the ensemble-averaged MSD (EA-MSD) to the time-averaged MSD (TA-MSD).[37,93] The TA-MSD is calculated for individual trajectories and follows the time dependent correlation function of each particle over time,

$$\overline{\delta_k^2}(\tau) = \frac{1}{T_k - \tau} \int_0^{T_k - \tau} (\vec{r}_k(t+\tau) - \vec{r}_k(t))^2 dt, \tag{2}$$

where $\tau$ is the lag time, $\vec{r}_k(t)$ is the position of the $k$th particle at time $t$, $T_k$ is the duration of the $k$th trajectory, and $t$ is the integration variable for the temporal averaging. However, due to experimental limitations, the trajectories of the particles are not long enough to obtain good reliable data at $\tau > 0.5$ s. Therefore, we calculate the ensemble-average of the TA-MSD curves of all particles to obtain the TEA-MSD of all trajectories and compare it to that of the EA-MSD. The TEA-MSD is defined as

$$\langle \overline{\delta_k^2}(\tau) \rangle \equiv \frac{1}{N_\tau} \sum_{k=1}^{N_\tau} \overline{\delta_k^2}(\tau), \tag{3}$$

where $N_\tau$ is the number of trajectories spanning a time lag greater than $\tau$. We note that as $\tau$ increases, these two plots should converge since the TEA-MSD is dominated by the time-average at small $\tau$ and by the ensemble-average at large $\tau$. In Figs. 3(a)–3(c), we show both the EA-MSD and the TEA-MSD of samples with $a/\xi = 0.26$, 0.79, and 0.88, corresponding to three regimes of different behaviors. Clearly, only for $a/\xi = 0.79$, the diffusion is non-ergodic. As expected, the difference is more pronounced for smaller lag times where the time average in the TEA-MSD curves dominates the ensemble-average. Therefore, we chose to evaluate ergodicity from the difference in the value of the EA-MSD and TEA-MSD at $\tau = 0.1$ s for different a/ξ values, as shown in Fig. 3(d). We identify three distinct regimes: normal-like diffusion at $a/\xi < 0.4$, CTRW-like diffusion at $0.4 < a/\xi < 0.8$, and an ergodic sub-diffusion process (fBm or another ergodic mechanism) at $0.8 < a/\xi < 1$.[5]

Finally, in order to decide whether the tracer particles diffuse in actin networks in the range of $a/\xi > 0.8$, according to fBm or another mechanism, we extracted the step-size probability distribution function (PDF) from their trajectories at different lag times and fitted it to a Gaussian curve, which is the final test suggested in Refs. 5 and 37. In Figs. 4(a)–4(c), we show typical PDFs for samples in the three regimes. We then proceed to evaluate the Gaussianity of the PDFs for all samples at all lag times using the non-Gaussian parameter (NGP), which is given by

$$\mathrm{NGP}(\tau) = \frac{\overline{\langle \Delta x(\tau)^4 \rangle}}{3\overline{\langle \Delta x(\tau)^2 \rangle}^2} - 1, \tag{4}$$

where $\Delta x(\tau)$ is the projected displacement on one axis ($\hat{x}$ or $\hat{y}$) within a time window of $\tau$ averaged over both time and ensemble. The NGP represents the deviation of the kurtosis from the Gaussian value and approaches zero for Gaussian distributions.[94] The lag time dependence of the NGP for different values of a/ξ is depicted in Fig. 4(d). For $a/\xi = 0.26$, we find a close value to the Gaussian PDF at all lag times. This further confirms that the diffusion in this regime is normal with no considerable effect of confinement by the network. For the second regime, where $0.56 \le a/\xi \le 0.79$, we find that the PDF is not Gaussian at all time scales. The deviation from a Gaussian

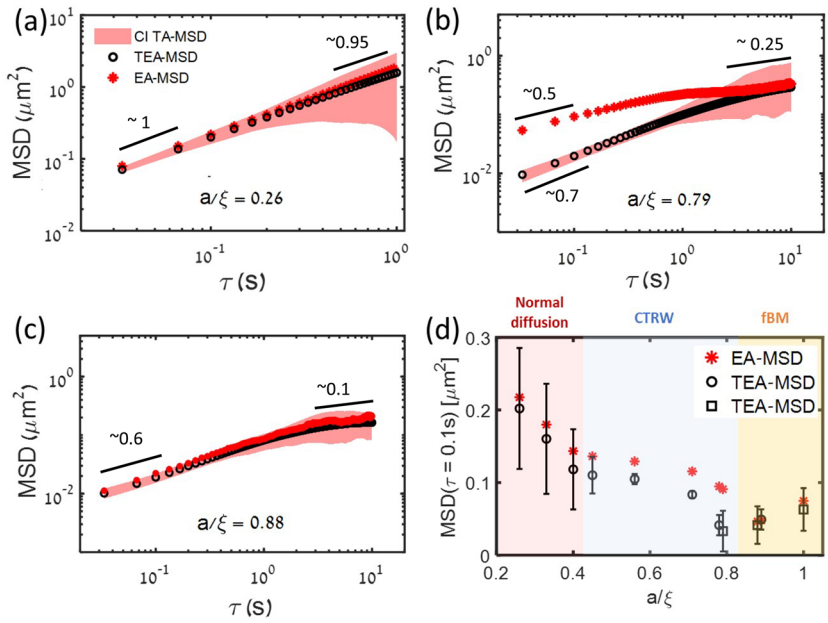


**FIG. 3**. Comparison between the EA-MSD and the TEA-MSD of individual probe particles for (a) $a/\xi = 0.26$, (b) $a/\xi = 0.79$, and (c) $a/\xi = 0.88$. The pink shadow indicates the confidence interval (CI) for the calculated TA-MSD. (d) The value of the MSD at $\tau = 0.1$ s for actin networks with ratios of the probe bead's radius to the mesh size in the range of $0.26 \leq a/\xi \leq 1$. Black circles and squares refer to a = 0.25 and 0.75 $\mu$m probe particles, respectively, and error bars indicate the 85% CI for the calculated TEA-MSD. The errors for the EA-MSD are smaller than the symbol size. Background color separation demonstrates the transition from a non-ergodic (white background) to an ergodic (pink and yellow background) process.

PDF cannot uniquely explain the mechanism of the dynamics and is expected due to the considerable effect of confinement by the actin network. For the last measured regime, where $0.8 < a/\xi < 1$, we find that the deviation from the Gaussian PDF is smaller (than the deviation found for the second regime) for long time lags. This is in agreement with the fact that for large $a/\xi$ ratios, the tracer particles only visited a few cages.

As already demonstrated in Figs. 1(c)–1(e), at intermediate values of $a/\xi$, particles jump randomly between different micro-environments in which they are constrained. This can be seen more convincingly when plotting the trajectory in 3D with time as the $z$ axis [see Figs. 5(a) and 5(b)]. Such dynamics can be characterized by the probability distribution of caging times $P(\tau_c)$ within the local micro-environments, which according to CTRW theory, should be

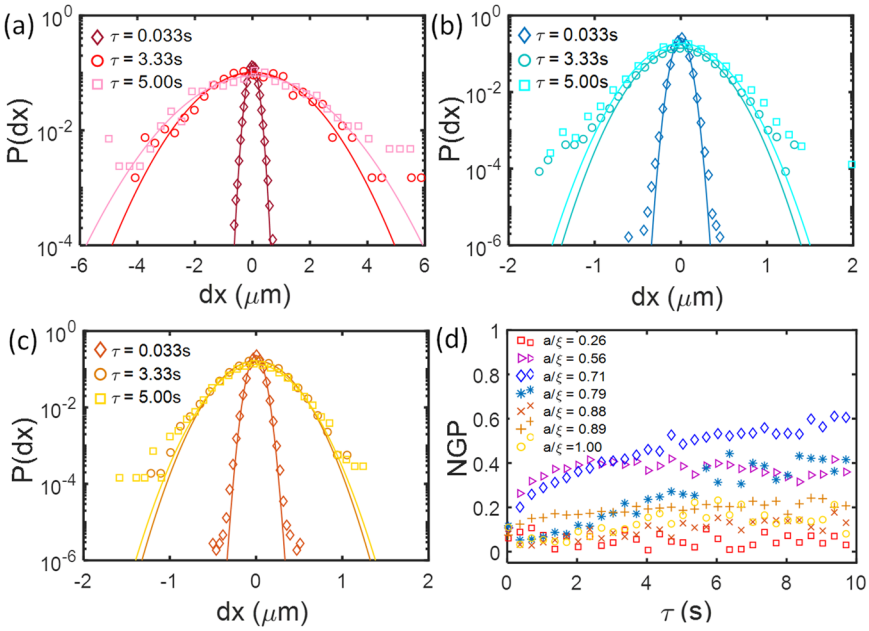


**FIG. 4**. PDF for different lag times for the ratio of the probe bead's radius to the mesh size of (a) $a/\xi = 0.26$, (b) $a/\xi = 0.79$, and (c) $a/\xi = 0.88$. Colored lines indicate a Gaussian fit to the short and long lag times. (d) The NGP as a function of $\tau$ for actin networks with ratios of the probe bead's radius to the mesh size within the range of $0.26 \leq a/\xi \leq 1$.

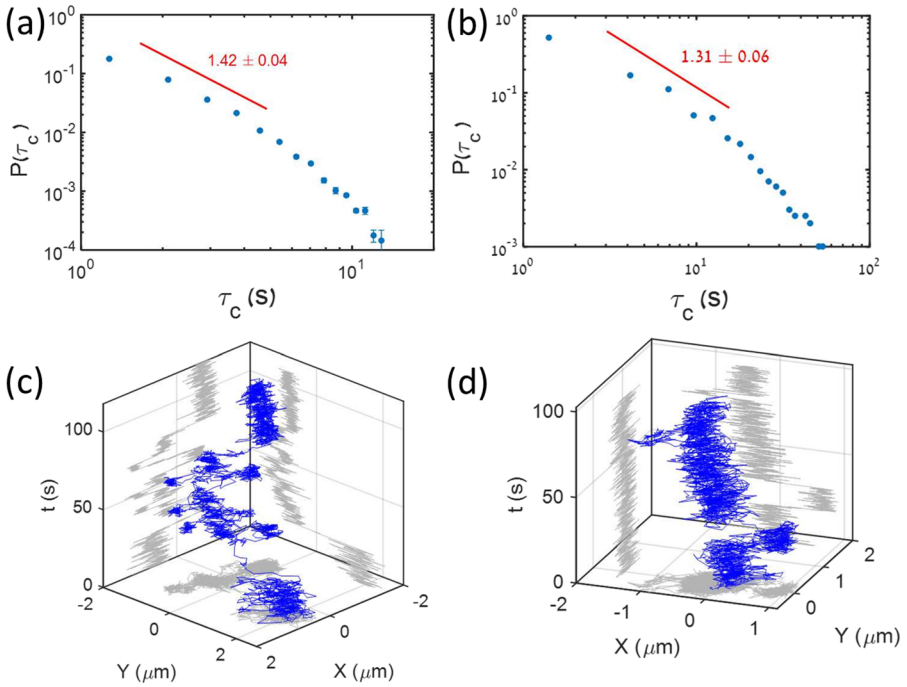


**FIG. 5**. Histogram of caging times for diffusing particles in an entangled F-actin network with particle radius to mesh size ratios of (a) a/ξ = 0.71 and (b) a/ξ = 0.78. The red line indicates a power-law fit, $P(\tau_c) \sim \tau_c^{-\nu}$, with $\nu$ = 1.42 ± 0.04 and 1.31 ± 0.06, respectively. (c) and (d) Representative trajectories of tracer particles projected on the x–y plane as a function of time for samples with a/ξ = 0.71 and 0.78, respectively.

scaled as a power-law with the caging time, i.e., $P(\tau_c) \sim \tau_c^{-\nu}$. We extract $P(\tau_c)$ directly from the trajectories by identifying the onset of caging and the escape. We then accumulate data from all the trajectories in the sample and plot it as a function of $\tau_c$. For example, we show the caging time distribution for a/ξ = 0.71 and a/ξ = 0.78 in Figs. 5(c) and 5(d). In these plots, we observe that at larger values of $\tau_c$, the power-law decreases, possibly due to the lack of sufficient statistics (in accord with Ref. 60). We, therefore, extract the power-law from the slope at small $\tau_c$.

The CTRW model describes anomalous diffusion arising from random walks with discrete steps of constant velocity, separated by pauses of random duration. When the direction of the random steps is chosen symmetrically and $1 < \nu < 2$, CTRW predicts that the MSD should be sub-diffusive, scaling asymptotically as $\alpha = \nu - 1$ for uncorrelated jumps.[95,96] In order to test the validity of the relation between the diffusion exponent and the caging power-law, we calculated $P(\tau_c)$ for all a/ξ values and extracted the power-law, $\nu$. In Fig. 6, we plot $\nu$ as a function of $\alpha + 1$. The three diffusion regimes are clearly observed in this analysis, confirming that for 0.4 < a/ξ < 0.8, particles diffuse in a CTRW-like process. Figure 6 shows a summary of all the diffusion mechanisms that were revealed for the tracer particles in the entangled actin network for the whole range of 0.26 ≤ a/ξ ≤ 1 studied here. It is important to note that for the CTRW-like regime, we tested the data for an aging signature expected for a CTRW.[97] However, we could not identify any signatures of aging over the time scale of the measurements.

We propose caged fBm as a conceptual model for the tracer dynamics in actin networks observed here. The viscoelastic response of the actin network to perturbations induced by the thermal motion of the tracer particle is long lived and has memory. This response will induce an fBm of the tracer particle when it is large enough to have almost continuous contact with the filaments (i.e., when $a/\xi > 0.5$). However, the filaments also confine the motion of the tracer. Long range motion is possible only when the tracer hops between cages formed by the actin filaments. The suggested model is a

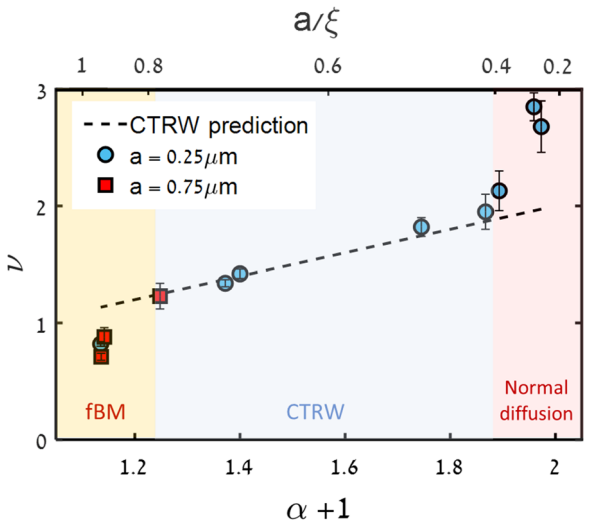


**FIG. 6**. Power-law fit value ($\nu$), extracted from the relation $P(\tau_c) \sim \tau_c^{-\nu}$ for ratios of the probe bead radius to the actin network's mesh size in the range of 0.26 ≤ a/ξ ≤ 1, vs the observed diffusion exponent plus one ($\alpha$ + 1). For CTRW, we expect $\nu = \alpha + 1$. Only within the range 0.4 < a/ξ < 0.8, there is good agreement with CTRW theory, while for lower and larger ratios, there are significant deviations that indicate that the diffusion is dominated by other mechanisms. Based on the results obtained previously, we can deduce that these diffusion mechanisms are fBm for a/ξ > 0.8 and free diffusion for 0.26 < a/ξ < 0.4.

subordinated fBm[98] due to the caging by the actin filaments. For this type of dynamics, one expects a transition from an fBm for short times while the tracer is mostly within a cage to different longer time dynamics that is dictated by the distribution of the caging times (or escape times). For a caging time distribution with finite moments, the long time asymptotic is a normal diffusion (the mean escape time of a particle undergoing fBm is finite), and for a power-law distribution of caging times with diverging first moment, the long time dynamics is characterized by a CTRW induced anomalous diffusion. We found that the cage size distribution is relatively narrow and that there is no correlation between the cage size and the escape time from the cage. These two properties hint that the escape and caging depend on the large bending fluctuations of actin filaments that release the trapped tracer. To test our proposed model, we simulated two variants of the caged fBm model: with power-law and exponential distributions of the caging times. For each distribution, we simulated 1000 trajectories. The model is not a microscopic model but rather a conceptual one. Each of the simulated trajectories is composed of a series of correlated jumps corresponding to fBm. The 1D space is split into cages with sizes distributed according to a gamma distribution, with the average cage size set to 0.6 $\mu$m (motivated by the measured cage size distribution, we set the scale parameter to 5 $\mu$m and the shape parameter to 0.12). For each cage, a random escape time is drawn (either exponentially distributed or power-law distributed), and the cage boundaries act as reflecting boundaries for the duration of the caging time. Once the particle escapes the cage and enters a neighboring cage, the fBm continues as usual, but the particle is subjected to the boundary conditions of the new cage. The time step was set to 1/30 s, the standard deviation of the step-size was set to 0.4 $\mu$m, and the Hurst exponent was 0.25. For the exponentially distributed caging times, we used the following PDF: $f(\tau_c) = (1/\tau_0)\exp(-\tau_c/\tau_0)$ with $\tau_0 = 33.3$ s. For the power-law distributed caging times we used, $f(\tau_c) = 0.18\alpha\tau_0^{\alpha}/\tau_c^{1+\alpha}$ with $\alpha = 0.5$. The results are presented in Fig. 7. Based on experimental evidence, we used a gamma distribution of cage sizes. This was the source of the different TA-MSDs in the case of the exponentially distributed caging time. For the power-law distributed caging time, the TA-MSD is a random variable, and the TEA-MSD is not equal to the EA-MSD due to the ergodicity breaking. In both cases, the short time behavior is dictated by the fBm while the long time behavior is different between the two cases, as described above. The measured dynamics appear to be similar to the results for a caged fBm with a power-law distribution of caging times. The supporting characteristics are the fact that the spread of the TA-MSDs does not seem to grow over time (before the number of trajectories becomes very small) and the fact that the EA-MSD is larger than the TEA-MSD at intermediate times. However, for the measured data, there are limitations (there is a smaller number of long trajectories, and the statistics at long lag times are dominated by the ensemble average) that do not exist for the simulated trajectories. Therefore, the results are not expected to fully coincide.

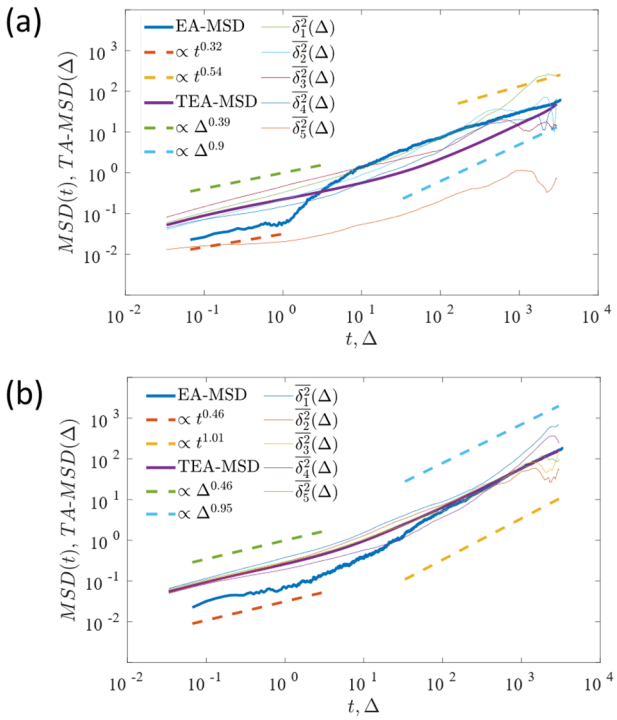


**FIG. 7**. Simulated ensemble-averaged square displacement (EA-MSD), ensemble-average of time-averaged square displacement (TEA-MSD), and time-averaged square displacements (TA-MSD): (a) caged fBm with power-law distributed caging times and (b) caged fBm with exponentially distributed caging times. For both cases, there is a clear transition between the short time (within the cage) and the long time (including hoping between cages) dynamics. The solid lines represent the EA-MSD and the TEA-MSD, respectively; the dashed lines represent the fitted power-law curves; and the thin solid lines represent the TA-MSD of typical trajectories. The simulation parameters are provided in the text. The MSD units are $(\mu m)^2$, and the time units are seconds.

## IV. CONCLUDING REMARKS

Our results suggest that the diffusion characteristics of the tracer particles are considerably affected by the ratio a/$\xi$ in the regime where the sizes of the tracer particle and the network mesh are comparable (a ~ $\xi$). We observed that the surprising CTRW-like motion of tracer particles in an *in vitro* polymerized actin network belongs to one of the three diffusion mechanisms that are seen in these networks. For small ratios, the particles perform normal diffusion through the network pores; at intermediate ratio values, they perform CTRW-like motion; and at large ratios, they perform fBm, as was originally expected. The physical processes leading to the diffusion at high and low ratio values are well understood; however, the physical reasons for the CTRW-like motion at intermediate values of a/$\xi$ are not clear. Clearly, the tracer particles at these conditions hop between adjacent compartments within the network [Figs. 5(c) and 5(d)]. However, the physical reason for a power-law distribution of escape times from a compartment [at least at short times, Figs. 5(a) and 5(b)] is yet to be determined.

It is tempting to try and describe the dynamics as a sequence of escapes from cages. For small tracer particles, one would naively assume that dynamics within the compartment are simply a normal diffusion (with a probably reduced diffusivity, as indeed observed, due to the hydrodynamic effects imposed by the network). For normal diffusion, the mean escape time from a cage is finite and scales

as the square of the cage size divided by the diffusion coefficient. Therefore, assuming that the cage does not change much during the measurement time, one would simply expect a transition between diffusion within the cage at short times and diffusion between cages at long times (note that if the caging/trapping is not significant, the diffusivity within the cage and between cages is expected to be very similar). Moreover, the probability distribution of escape times (or residence times within the cage) is expected to have an exponentially decaying tail. Note that this type of dynamics resembles the observed dynamics for a small ratio of a/ξ.

For tracer particles of a size similar to the network mesh size, the interaction of the particle with the network filaments is expected to induce fBm dynamics. For a particle exhibiting fBm, the mean escape time from a cage scales from the size of the cage to the power $2/\alpha$ ($0 \leq \alpha \leq 1$ is the diffusion exponent).[99] The probability density function of the escape time is expected to have a stretched exponent decaying tail. Nevertheless, all the moments of the escape time are finite, and the dynamics over long time scales are expected to exhibit normal diffusion. There is no evidence for a broad distribution of cage sizes that may result in a CTRW. Therefore, the origin of the CTRW-like dynamics is likely to be the interaction between the tracer particle and the actin filaments that triggers the large bending of the actin filaments, thereby enabling the escape from the cage. It is also important to note that for a CTRW, the TA-MSD is expected to be linear with the lag time (unlike the EA-MSD). However, our results show that it is not. Moreover, we did not find any evidence for aging, as expected for a CTRW. The power-law waiting time PDF and its correspondence with the diffusion exponent support the CTRW dynamics. A possible explanation for the discrepancies between CTRW and the observed dynamics may be the fact that our trajectories span a relatively small number of cages, and therefore, the dynamics are not expected to converge to the asymptotic limit of CTRW.

Our simulation results show that anomalous diffusion may be exhibited by particles undergoing caged fBm regardless of the distribution of the caging times. The TA-MSD of individual tracers may be different due to the heterogeneity of the cage sizes (even when the distribution is narrow) and the finite duration of the measurement. However, in order to tightly relate the model to the experiment, one has to understand the mechanism of escaping from the actin cage, as in Ref. 100.

In our analysis, we analyzed trajectories of approximately equal and relatively long length (2000 frames ≈67 s). This was carried out to allow for an equal and sufficient amount of statistics in each analysis. Long trajectories are commonly required to compare measurements to the asymptotic behavior described in the theoretical model. In many experimental scenarios, long trajectories are unavailable due to technical issues such as finite fluorescence lifetime of tagged molecules or due to fast or changing dynamics of the tracer particles. Therefore, there is a need to develop alternative classification schemes for diffusion processes that can be obtained from relatively short trajectories and can be tied to the underlying physics. Here, we used the step-size distribution that could be extracted from a large ensemble on shorter trajectories; similarly, to some extent, the escape time distribution up to a given cutoff can be obtained from such an ensemble. This is a first step toward such a new classification.

One important implication of our results is related to the characterization of biological systems and processes using single molecule tracking. Specifically, the type of motion of a tracer particle, or a molecule, in a complex material depends dramatically on the relation between its size and the typical length scales of the material. One approach to overcome this challenge can be to use tracers of different sizes. An alternative powerful tool would be to use the correlations in the motion of the tracer particles, as carried out in two-point microrheology.[101] The correlated diffusion carries structural information[47,59,102] even when applied to systems out of thermal equilibrium.[55]

## SUPPLEMENTARY MATERIAL

See the supplementary material for a comparison between the EA-MSD, TEA-MSD, and TA-MSD of individual probe particles of different sizes, as well as trajectories in three dimensional representation and fitting of the PDFs for the CTRW-dominated part.

## ACKNOWLEDGMENTS

The authors are grateful to Anne Bernheim-Groswasser for the numerous discussions and for providing actin. M.L. and Y.R. thank the Center for Light Matter Interaction in Tel-Aviv University for its support. This work was partially supported by the US-Israel Binational Science Foundation (Grant No. 2014314) and the ISF (Israel Science Foundation) (Grant No. 988/17).

## DATA AVAILABILITY

The data that support the findings of this study are available from the corresponding author upon reasonable request.

## REFERENCES

[1] S. Shashkova and M. C. Leake, "Single-molecule fluorescence microscopy review: Shedding new light on old problems," Biosci. Rep. **37**, BSR20170031 (2017).
[2] S. Hou, C. Johnson, and K. Welsher, "Real-time 3D single particle tracking: Towards active feedback single molecule spectroscopy in live cells," Molecules **24**, 2826 (2019).
[3] S.-L. Liu, Z.-L. Zhang, E.-Z. Sun, J. Peng, M. Xie, Z.-Q. Tian, Y. Lin, and D.-W. Pang, "Visualizing the endocytic and exocytic processes of wheat germ agglutinin by quantum dot-based single-particle tracking," Biomaterials **32**, 7616–7624 (2011).
[4] R. Hao, Z. Peng, and B. Zhang, "Single-molecule fluorescence microscopy for probing the electrochemical interface," ACS Omega **5**, 89–97 (2020).
[5] Y. Meroz and I. M. Sokolov, "A toolbox for determining subdiffusive mechanisms," Phys. Rep. **573**, 1–29 (2015).
[6] A. I. König, R. Sorkin, A. Alon, D. Nachmias, K. Dhara, G. Brand, O. Yifrach, E. Arbely, Y. Roichman, and N. Elia, "Live cell single molecule tracking and localization microscopy of bioorthogonally labeled plasma membrane proteins," Nanoscale **12**, 3236–3248 (2020).
[7] Y. Han and D. G. Grier, "Configurational temperatures and interactions in charge-stabilized colloid," J. Chem. Phys. **122**, 064907 (2005).
[8] C. Holm, P. Kékicheff, and R. Podgornik, *Electrostatic Effects in Soft Matter and Biophysics* (Springer Science & Business Media, 2001), Vol. 46.
[9] B. Cui, H. Diamant, B. Lin, and S. A. Rice, "Anomalous hydrodynamic interaction in a quasi-two-dimensional suspension," Phys. Rev. Lett. **92**, 258301 (2004).
[10] O. Tal-Friedman, A. Pal, A. Sekhon, S. Reuveni, and Y. Roichman, "Experimental realization of diffusion with stochastic resetting," J. Phys. Chem. Lett. **11**, 7350–7355 (2020).

[11]T. Admon, S. Rahav, and Y. Roichman, "Experimental realization of an information machine with tunable temporal correlations," Phys. Rev. Lett. **121**, 180601 (2018).
[12]A. Bérut, A. Arakelyan, A. Petrosyan, S. Ciliberto, R. Dillenschneider, and E. Lutz, "Experimental verification of Landauer's principle linking information and thermodynamics," Nature **483**, 187–189 (2012).
[13]M. Ribezzi-Crivellari and F. Ritort, "Large work extraction and the Landauer limit in a continuous Maxwell demon," Nat. Phys. **15**, 660–664 (2019).
[14]I. M. Sokolov, "Models of anomalous diffusion in crowded environments," Soft Matter **8**, 9043–9052 (2012).
[15]R. Metzler, J.-H. Jeon, A. G. Cherstvy, and E. Barkai, "Anomalous diffusion models and their properties: Non-stationarity, non-ergodicity, and ageing at the centenary of single particle tracking," Phys. Chem. Chem. Phys. **16**, 24128–24164 (2014).
[16]N. Granik, L. E. Weiss, E. Nehme, M. Levin, M. Chein, E. Perlson, Y. Roichman, and Y. Shechtman, "Single-particle diffusion characterization by deep learning," Biophys. J. **117**, 185–192 (2019).
[17]S. Bo, F. Schmidt, R. Eichhorn, and G. Volpe, "Measurement of anomalous diffusion using recurrent neural networks," Phys. Rev. E **100**, 010102 (2019).
[18]G. Muñoz-Gil, M. A. Garcia-March, C. Manzo, J. D. Martín-Guerrero, and M. Lewenstein, "Single trajectory characterization via machine learning," New J. Phys. **22**, 013010 (2020).
[19]P. Kowalek, H. Loch-Olszewska, and J. Szwabiński, "Classification of diffusion modes in single-particle tracking data: Feature-based versus deep-learning approach," Phys. Rev. E **100**, 032410 (2019).
[20]R. Vangara, K. Ø. Rasmussen, D. N. Petsev, G. Bel, and B. S. Alexandrov, "Identification of anomalous diffusion sources by unsupervised learning," Phys. Rev. Res. **2**, 023248 (2020).
[21]S. Thapa, M. A. Lomholt, J. Krog, A. G. Cherstvy, and R. Metzler, "Bayesian analysis of single-particle tracking data using the nested-sampling algorithm: Maximum-likelihood model selection applied to stochastic-diffusivity data," Phys. Chem. Chem. Phys. **20**, 29018–29037 (2018).
[22]D. Krapf, E. Marinari, R. Metzler, G. Oshanin, X. Xu, and A. Squarcini, "Power spectral density of a single Brownian trajectory: What one can and cannot learn from it," New J. Phys. **20**, 023029 (2018).
[23]A. G. Cherstvy, S. Thapa, C. E. Wagner, and R. Metzler, "Non-Gaussian, non-ergodic, and non-Fickian diffusion of tracers in mucin hydrogels," Soft Matter **15**, 2526–2551 (2019).
[24]A. Sabri, X. Xu, D. Krapf, and M. Weiss, "Elucidating the origin of heterogeneous anomalous diffusion in the cytoplasm of mammalian cells," Phys. Rev. Lett. **125**, 058101 (2020).
[25]C. E. Wagner, B. S. Turner, M. Rubinstein, G. H. McKinley, and K. Ribbeck, "A rheological study of the association and dynamics of MUC5AC gels," Biomacromolecules **18**, 3654–3664 (2017).
[26]E. Yamamoto, T. Akimoto, M. Yasui, and K. Yasuoka, "Origin of subdiffusion of water molecules on cell membrane surfaces," Sci. Rep. **4**, 4720 (2015).
[27]M. Weiss, M. Elsner, F. Kartberg, and T. Nilsson, "Anomalous subdiffusion is a measure for cytoplasmic crowding in living cells," Biophys. J. **87**, 3518–3524 (2004).
[28]H. Berry and H. A. Soula, "Spatial distributions at equilibrium under heterogeneous transient subdiffusion," Front. Physiol. **5**, 437 (2014).
[29]L. Silvestri, L. Fronzoni, P. Grigolini, and P. Allegrini, "Event-driven power-law relaxation in weak turbulence," Phys. Rev. Lett. **102**, 014502 (2009).
[30]K. Maeda, T. Narumi, R. Anugraha, H. Okabe, K. Hara, and Y. Hidaka, "Subdiffusion in electroconvective turbulence of homeotropic nematic liquid crystals," J. Phys. Soc. Jpn. **87**, 014401 (2018).
[31]C. J. Weiss and M. E. Everett, "Anomalous diffusion of electromagnetic eddy currents in geological formations," J. Geophys. Res. **112**, B08102, https://doi.org/10.1029/2006jb004475 (2007).
[32]Y. Wang, "Anomalous transport in weakly heterogeneous geological porous media," Phys. Rev. E **87**, 032144 (2013).
[33]S. Condamin, V. Tejedor, R. Voituriez, O. Bénichou, and J. Klafter, "Probing microscopic origins of confined subdiffusion by first-passage observables," Proc. Natl. Acad. Sci. U. S. A. **105**, 5675–5680 (2008).
[34]H. Scher and E. W. Montroll, "Anomalous transit-time dispersion in amorphous solids," Phys. Rev. B **12**, 2455–2477 (1975).
[35]I. Golding and E. C. Cox, "Physical nature of bacterial cytoplasm," Phys. Rev. Lett. **96**, 098102 (2006).
[36]J.-H. Jeon, N. Leijnse, L. B. Oddershede, and R. Metzler, "Anomalous diffusion and power-law relaxation of the time averaged mean squared displacement in worm-like micellar solutions," New J. Phys. **15**, 045011 (2013).
[37]Y. Meroz, I. M. Sokolov, and J. Klafter, "Test for determining a subdiffusive model in ergodic systems from single trajectories," Phys. Rev. Lett. **110**, 090601 (2013).
[38]J. Klafter, A. Blumen, and G. Zumofen, "Fractal behavior in trapping and reaction: A random walk study," J. Stat. Phys. **36**, 561–577 (1984).
[39]V. Balakrishnan, "Random walks on fractals," Mater. Sci. Eng., B **32**, 201–210 (1995), containing papers presented at the Indo-US Workshop on Nucleation and Growth in Solids.
[40]J. Rogel-Salazar, "First steps in random walks: From tools to applications, by J. Klafter and I.M. Sokolov," Contemp. Phys. **53**, 369–370 (2012).
[41]J.-P. Bouchaud and A. Georges, "Anomalous diffusion in disordered media: Statistical mechanisms, models and physical applications," Phys. Rep. **195**, 127–293 (1990).
[42]S. Burov and E. Barkai, "Time transformation for random walks in the quenched trap model," Phys. Rev. Lett. **106**, 140602 (2011).
[43]B. B. Mandelbrot and J. W. Van Ness, "Fractional Brownian motions, fractional noises and applications," SIAM Rev. **10**, 422–437 (1968).
[44]M. Maejima and C. Tudor, "Selfsimilar processes with stationary increments in the second Wiener chaos," Probab. Math. Stat. **32**, 167–186 (2012).
[45]L. Decreusefond and A. Ustunel, "Fractional Brownian motion: Theory and applications," ESAIM: Proc. **5**, 75–86 (1999).
[46]M. L. Gardel, M. T. Valentine, J. C. Crocker, A. R. Bausch, and D. A. Weitz, "Microrheology of entangled F-actin solutions," Phys. Rev. Lett. **91**, 158302 (2003).
[47]J. Liu, M. L. Gardel, K. Kroy, E. Frey, B. D. Hoffman, J. C. Crocker, A. R. Bausch, and D. A. Weitz, "Microrheology probes length scale dependent rheology," Phys. Rev. Lett. **96**, 118104 (2006).
[48]M. L. Gardel, K. E. Kasza, C. P. Brangwynne, J. Liu, and D. A. Weitz, "Chapter 19: Mechanical response of cytoskeletal networks," Methods Cell Biol. **89**, 487–519 (2008).
[49]J. Stricker, T. Falzone, and M. Gardel, "Mechanics of the F-actin cytoskeleton," J. Biomech. **43**, 9–14 (2009).
[50]D. Sept, J. Xu, T. D. Pollard, and J. Andrew McCammon, "Annealing accounts for the length of actin filaments formed by spontaneous polymerization," Biophys. J. **77**, 2911–2919 (1999).
[51]J. A. Cooper, S. B. Walker, and T. D. Pollard, "Pyrene actin: Documentation of the validity of a sensitive assay for actin polymerization," J. Muscle Res. Cell Motil. **4**, 253–262 (1983).
[52]S. Z. Chou and T. D. Pollard, "Mechanism of actin polymerization revealed by cryo-EM structures of actin filaments with three different bound nucleotides," Proc. Natl. Acad. Sci. U. S. A. **116**, 4265–4274 (2019).
[53]J. H. Shin, M. L. Gardel, L. Mahadevan, P. Matsudaira, and D. A. Weitz, "Relating microstructure to rheology of a bundled and cross-linked F-actin network *in vitro*," Proc. Natl. Acad. Sci. U. S. A. **101**, 9636–9641 (2004).
[54]L. Haviv, N. Gov, Y. Ideses, and A. Bernheim-Groswasser, "Thickness distribution of actin bundles in vitro," Eur. Biophys. J. **37**, 447–454 (2008).
[55]A. Sonn-Segev, A. Bernheim-Groswasser, and Y. Roichman, "Dynamics in steady state *in vitro* acto-myosin networks," J. Condens. Matter Phys. **29**, 163002 (2017).
[56]H. Lee, J. M. Ferrer, F. Nakamura, M. J. Lang, and R. D. Kamm, "Passive and active microrheology for cross-linked F-actin networks *in vitro*," Acta Biomater. **6**, 1207–1218 (2010).
[57]A. Palmer, T. G. Mason, J. Y. Xu, S. C. Kuo, and D. Wirtz, "Diffusing wave spectroscopy microrheology of actin filament networks," Biophys. J. **76**, 1063–1071 (1999).
[58]A. Sonn Segev, A. Bernheim, and Y. Roichman, "Extracting the dynamic correlation length of actin networks from microrheology experiments," Soft Matter **10**, 8324 (2014).

[59]A. Sonn-Segev, A. Bernheim-Groswasser, H. Diamant, and Y. Roichman, "Viscoelastic response of a complex fluid at intermediate distances," Phys. Rev. Lett. **112**, 088301 (2014).
[60]I. Y. Wong, M. L. Gardel, D. R. Reichman, E. R. Weeks, M. T. Valentine, A. R. Bausch, and D. A. Weitz, "Anomalous diffusion probes microstructure dynamics of entangled F-actin networks," Phys. Rev. Lett. **92**, 178101 (2004).
[61]S. K. Ghosh, A. G. Cherstvy, and R. Metzler, "Non-universal tracer diffusion in crowded media of non-inert obstacles," Phys. Chem. Chem. Phys. **17**, 1847–1858 (2015).
[62]A. S. Verkman, "Solute and macromolecule diffusion in cellular aqueous compartments," Trends Biochem. Sci. **27**, 27–33 (2002).
[63]M. Magdziarz, A. Weron, K. Burnecki, and J. Klafter, "Fractional Brownian motion versus the continuous-time random walk: A simple test for subdiffusive dynamics," Phys. Rev. Lett. **103**, 180602 (2009).
[64]S. C. Weber, A. J. Spakowitz, and J. A. Theriot, "Bacterial chromosomal loci move subdiffusively through a viscoelastic cytoplasm," Phys. Rev. Lett. **104**, 238102 (2010).
[65]J.-H. Jeon, V. Tejedor, S. Burov, E. Barkai, C. Selhuber-Unkel, K. Berg-Sørensen, L. Oddershede, and R. Metzler, "*In vivo* anomalous diffusion and weak ergodicity breaking of lipid granules," Phys. Rev. Lett. **106**, 048103 (2011).
[66]K. Burnecki, E. Kepten, J. Janczura, I. Bronshtein, Y. Garini, and A. Weron, "Universal algorithm for identification of fractional Brownian motion. A case of telomere subdiffusion," Biophys. J. **103**, 1839–1847 (2012).
[67]D. Ernst, M. Hellmann, J. Köhler, and M. Weiss, "Fractional Brownian motion in crowded fluids," Soft Matter **8**, 4886–4889 (2012).
[68]J. Szymanski and M. Weiss, "Elucidating the origin of anomalous diffusion in crowded fluids," Phys. Rev. Lett. **103**, 038102 (2009).
[69]J. Sprakel, J. van der Gucht, M. A. Cohen Stuart, and N. A. M. Besseling, "Rouse dynamics of colloids bound to polymer networks," Phys. Rev. Lett. **99**, 208301 (2007).
[70]G. Guigas and M. Weiss, "Sampling the cell with anomalous diffusion—The discovery of slowness," Biophys. J. **94**, 90–94 (2008).
[71]S. Joo, X. Durang, O.-c. Lee, and J.-H. Jeon, "Anomalous diffusion of active Brownian particles cross-linked to a networked polymer: Langevin dynamics simulation and theory," Soft Matter **16**, 9188–9201 (2020).
[72]H. Diamant, "Response of a polymer network to the motion of a rigid sphere," Eur. Phys. J. E **38**, 32 (2015).
[73]L.-H. Cai, S. Panyukov, and M. Rubinstein, "Hopping diffusion of nanoparticles in polymer matrices," Macromolecules **48**, 847–862 (2015).
[74]J. A. Spudich and S. Watt, "The regulation of rabbit skeletal muscle contraction," J. Biol. Chem. **246**, 4866–4871 (1971).
[75]M. T. Valentine, Z. E. Perlman, M. L. Gardel, J. H. Shin, P. Matsudaira, T. J. Mitchison, and D. A. Weitz, "Colloid surface chemistry critically affects multiple particle tracking measurements of biomaterials," Biophys. J. **86**, 4004–4014 (2004).
[76]C. F. Schmidt, M. Baermann, G. Isenberg, and E. Sackmann, "Chain dynamics, mesh size, and diffusive transport in networks of polymerized actin: A quasielastic light-scattering and microfluorescence study," Macromolecules **22**, 3638–3649 (1989).
[77]M. Levin, R. Sorkin, D. Pine, R. Granek, A. Bernheim-Groswasser, and Y. Roichman, "Kinetics of actin networks formation measured by time resolved particle-tracking microrheology," Soft Matter **16**, 7869–7876 (2020).
[78]J. Liu, G. H. Koenderink, K. E. Kasza, F. C. MacKintosh, and D. A. Weitz, "Visualizing the strain field in semiflexible polymer networks: Strain fluctuations and nonlinear rheology of F-actin gels," Phys. Rev. Lett. **98**, 198304 (2007).
[79]F. Gittes and F. C. MacKintosh, "Dynamic shear modulus of a semiflexible polymer network," Phys. Rev. E **58**, R1241–R1244 (1998).
[80]G. H. Koenderink, M. Atakhorrami, F. C. MacKintosh, and C. F. Schmidt, "High-frequency stress relaxation in semiflexible polymer solutions and networks," Phys. Rev. Lett. **96**, 138307 (2006).
[81]O. Lieleg, M. M. A. E. Claessens, C. Heussinger, E. Frey, and A. R. Bausch, "Mechanics of bundled semiflexible polymer networks," Phys. Rev. Lett. **99**, 088102 (2007).
[82]M. M. A. E. Claessens, R. Tharmann, K. Kroy, and A. R. Bausch, "Microstructure and viscoelasticity of confined semiflexible polymer networks," Nat. Phys. **2**, 186–189 (2006).
[83]H. Sanabria and M. N. Waxham, "Transient anomalous subdiffusion: Effects of specific and nonspecific probe binding with actin gels," J. Phys. Chem. B **114**, 959–972 (2010).
[84]B. S. Chae and E. M. Furst, "Probe surface chemistry dependence and local polymer network structure in F-actin microrheology," Langmuir **21**, 3084–3089 (2005).
[85]R. Götter, K. Kroy, E. Frey, M. Bärmann, and E. Sackmann, "Dynamic light scattering from semidilute actin solutions: A study of hydrodynamic screening, filament bending stiffness, and the effect of tropomyosin/troponin-binding," Macromolecules **29**, 30–36 (1996).
[86]S. Ricketts, M. Francis, L. Farhadi, M. Rust, J. Ross, and R. Robertson-Anderson, "Varying crosslinking motifs drive the mesoscale mechanics of actin-microtubule composites," Sci. Rep. **9**, 12831 (2019).
[87]J. C. Crocker and D. G. Grier, "Methods of digital video microscopy for colloidal studies," J. Colloid Interface Sci. **179**, 298–310 (1996).
[88]A. P. Minton, "The influence of macromolecular crowding and macromolecular confinement on biochemical reactions in physiological media," J. Biol. Chem. **276**, 10577–10580 (2001).
[89]D. S. Clague and R. J. Phillips, "Hindered diffusion of spherical macromolecules through dilute fibrous media," Phys. Fluids **8**, 1720–1731 (1996).
[90]G. Bel and E. Barkai, "Weak ergodicity breaking in the continuous-time random walk," Phys. Rev. Lett. **94**, 240602 (2005).
[91]G. Bel and E. Barkai, "Random walk to a nonergodic equilibrium concept," Phys. Rev. E **73**, 016125 (2006).
[92]G. Bel and E. Barkai, "Occupation times and ergodicity breaking in biased continuous time random walks," J. Phys.: Condens. Matter **17**, S4287–S4304 (2005).
[93]J. Janczura and A. Weron, "Ergodicity testing for anomalous diffusion: Small sample statistics," J. Chem. Phys. **142**, 144103 (2015).
[94]A. Rahman, "Correlations in the motion of atoms in liquid argon," Phys. Rev. **136**, A405–A411 (1964).
[95]M. F. Shlesinger, "Asymptotic solutions of continuous-time random walks," J. Stat. Phys. **10**, 421–434 (1974).
[96]E. R. Weeks, J. S. Urbach, and H. L. Swinney, "Anomalous diffusion in asymmetric random walks with a quasi-geostrophic flow example," Physica D **97**, 291–310 (1996).
[97]J. H. P. Schulz, E. Barkai, and R. Metzler, "Aging effects and population splitting in single-particle trajectory averages," Phys. Rev. Lett. **110**, 020602 (2013).
[98]S. M. A. Tabei, S. Burov, H. Y. Kim, A. Kuznetsov, T. Huynh, J. Jureller, L. H. Philipson, A. R. Dinner, and N. F. Scherer, "Intracellular transport of insulin granules is a subordinated random walk," Proc. Natl. Acad. Sci. U. S. A. **110**, 4911–4916 (2013).
[99]T. Guggenberger, G. Pagnini, T. Vojta, and R. Metzler, "Fractional Brownian motion in a finite interval: Correlations effect depletion or accretion zones of particles near boundaries," New J. Phys. **21**, 022002 (2019).
[100]A. Godec, M. Bauer, and R. Metzler, "Collective dynamics effect transient subdiffusion of inert tracers in flexible gel networks," New J. Phys. **16**, 092002 (2014).
[101]J. C. Crocker, M. T. Valentine, E. R. Weeks, T. Gisler, P. D. Kaplan, A. G. Yodh, and D. A. Weitz, "Two-point microrheology of inhomogeneous soft materials," Phys. Rev. Lett. **85**, 888–891 (2000).
[102]N. Oppenheimer and H. Diamant, "In-plane dynamics of membranes with immobile inclusions," Phys. Rev. Lett. **107**, 258102 (2011).